X International Conference on Computational Methods in Marine Engineering
MARINE 2023
J. García-Espinosa, L. González, J.E. Gutiérrez & B. Serván-Camas (Eds)

Scale resolving simulation of bow thruster hydrodynamics

M. Kazemi[1*] and N. Kornev[1]

[1] Chair of Modeling and Simulation (LeMoS), University of Rostock, A.Einstein Str, 18059 Rostock, Germany, e-mail: mehrdad.kazemi@uni-rostock.de, web page: https://www.lemos.uni-rostock.de/
[*] Corresponding author: Mehrdad Kazemi, mehrdad.kazemi@uni-rostock.de

ABSTRACT

The paper presents results of application of scale resolving simulations (hybrid URANS/LES) to the bow thruster hydrodynamics with and without cavitation. The CFD results are verified and validated on the basis of EFD results for integral forces and pressure fluctuations. A substantial increase of thrust fluctuations on bow thruster propeller in comparison to conventional propellers behind full ships is demonstrated. Results were obtained for a bow thruster manufactured by Jastram GmbH & Co. KG.

Keywords: bow thruster; URANS; LES; hybrid method; cavitation; unsteady effects.

NOMENCLATURE

T	thrust [N]
T_{mean}	time averaged thrust [N]
$T' = T - T_{mean}$	thrust fluctuation [N]
$\tilde{T'}$	referred thrust fluctuation [-]
t	time [sec]
BPF	Blade Passing Frequency
CFD	Computational Fluid Dynamics
DDES	Detached Delayed Eddy Simulation
EFD	Experimental Fluid Dynamics
LES	Large Eddy Simulation
TKE	Turbulence Kinetic Energy
(U) RANS	(Unsteady) Reynolds Averaged Navier Stokes
SLH	Shielded Lemos Hybrid method
SST	Shear Stress Transport
AMI	Arbitrary mesh interface
δt	Time step

1. INTRODUCTION

The flow field in the tunnel of the bow thruster is complicated by flow separations near the tunnel entrance, cavitation, and complex interaction between different components of the bow thruster (nacelle, tunnel wall and ship hull). That is why numerical modeling of the flow in the bow thruster is much more difficult than many other problems of hydrodynamics of ship propulsors. The insufficient number

of available experimental data makes it difficult to validate the CFD models for bow thruster hydrodynamics. The number of published CFD studies is limited, especially for these reasons, although there are many practically important parameters that can be investigated with CFD: geometry and position of the propeller blades, length, and inlet/ outlet geometry of the tunnel, shape of the linings of the ship, protective grids and influence of the ship's speed.

Yu and Yang (2016) used the RANS equations to investigate the hydrodynamics of a bow thruster using the $k-\omega$ SST turbulence model. The influence of blade pitch and area was systematically investigated. A similar investigation with RANS was carried out by Yao and Yan (2012), in which the influence of various geometric parameters and the ship's speed on the efficiency of the bow thruster is studied. In the work of Ozdemir *et al.* (2008), CFD was used with the traditional RANS $k-\varepsilon$ model to find an optimal geometry of the bow thruster. It was demonstrated that CFD is a suitable tool for the design of the bow thruster. Brizzolara (2017) designed a new tunnel configuration and thoroughly investigated it with CFD. A new configuration has been designed, which for a given tunnel length makes it possible to use a smaller propeller that has the efficiency of a larger propeller with the ideal length to diameter ratio of two to three. The realizable-$k-\varepsilon$ type turbulence model was used. The propeller was modeled using the actuator-disk approach. The influence of the tunnel shape on the efficiency of the bow thruster in a bagger with the actuator-disk model and temporally and spatially resolved propeller was investigated by Mohan (2017). A very thorough experimental and CFD study of bow thruster hydrodynamics was performed by Shevtsov (2014). The experiment was performed in the cavitation tunnel of the Krylov Reseach Center. Experimental studies to assess the effect of the power supply device (a nacelle) during pulling and pushing operation on hydrodynamic characteristics of thruster, as well as evaluation of influence of different channel inlet and outlet designs on thruster operation mode were performed. The papers cited before focus on the steady effects. Unsteady effects including vibrations are considered by Ermolaev and Shevtsov (2018). This paper gives an overview of flow physics effects inside the thruster causing the vibration and measures to reduce it. In Bagrintsev *et al.* (2019) a three stage procedure is proposed to design the bow thruster propeller with account of unsteady effects. In the first stage, the blade number is selected to reduce the periodic forces. Then the pitch distribution is found to mitigate the risk of cavitation inception. In the second stage the skew distribution is determined to minimize the periodic forces both on the propeller and tunnel walls. Within the third stage unsteady loads on the propeller and pressure fluctuations on the tunnel wall are calculated in the given velocity field using the potential lifting surface theory. An essential reduction of pressure fluctuations on the tunnel walls is demonstrated in comparison with original propeller case.

The choice of CFD method depends on the specific task. For improving the efficiency of thrusters, the conventional RANS methods, e.g. $k-\omega$ SST model, are fully suitable. For the calculation of the pressure pulses on structures, hydroacoustic and the transient loads on the propeller, the scaling resolving models are required. The paper presents comparative analysis of pressure pulses and transient loads in bow thruster, manufactured by Jastram company, obtained using RANS and scale resolving hybrid unsteady RANS/LES models.

2. MATHEMATICAL MODEL

The mathematical model includes the continuity equation for the incompressible flow

$$\frac{\partial \overline{u}_i}{\partial x_i} = 0 \tag{1}$$

and the momentum equation,

$$\frac{\partial \overline{u}_i}{\partial t} + \frac{\partial (\overline{u}_i \overline{u}_j)}{\partial x_j} = -\frac{\partial \overline{p}^*}{\partial x_i} + \frac{\partial (\tau^l_{ij} + \tau^t_{ij})}{\partial x_j}, \tag{2}$$

written both for the velocity $\overline{u}_j$ and pressure $\overline{p}$. In RANS zones the overline means the Reynolds average, whereas in LES the spatial filtering. Here we use the standard notation of p^* for the pseudo-pressure and τ^l_{ij} and τ^t_{ij} for the laminar and turbulent stresses, respectively. Three following turbulent models were utilized for calculation of τ^t_{ij}: 1) RANS Model (k-ω SST) by Menter F. R. (1994). 2) Hybrid DDES (Detached Delayed Eddy Simulation) model by Shur *et al.* (2008). The DDES routine available in the OpenFOAM is based on the Spalart Allmaras (SA) and k-ω SST URANS turbulence models 3) Hybrid Model SLH developed in our works Kornev *et al.* (2011), Abbas *et al.* (2015) and Shevchuk and Kornev (2018).

The computational domain in our SLH model is dynamically (i.e. at each time step) subdivided into the LES and URANS regions. The key quantities of this decomposition are a certain length scale $\tilde{L}$ and the extended LES filter Δ, which are computed for each cell of the mesh. A cell of the mesh belongs to one area or the other, depending on the value of $\tilde{L}$ relative to Δ: if $\tilde{L} > \Delta$ then the cell is in the LES area, in other cases it is in the URANS region. The length L is determined from the formula of Kolmogorov and Prandtl, which is valid for high local Reynolds numbers in the wake area and on the outer boundary of the boundary layer:

$$L = k^{3/2}/\varepsilon f_d = \frac{\sqrt{k}}{0.09\omega} f_d \tag{3}$$

where k is the turbulence kinetic energy, ε is the dissipation rate and ω is the specific dissipation rate. Introduction of shielding f_d in Shevchuk and Kornev (2018) was necessary to force the RANS/LES interface to move farther from the wall and to reduce the grid induced separation in a way which is analogous to transformation of DES to DDES. The shielding function was taken from DDES.

The turbulent stress τ^t_{ij} is calculated from the Boussinesq approximation using the concept of the turbulent viscosity which is considered as the subgrid viscosity in the LES region. The stress is computed according to the localized dynamic model of Smagorinsky in the LES region and according to the k-ω SST turbulence model of Menter (1994) in the URANS region. The wall functions are utilized in the near wall URANS region. The hybrid SLH model was thoroughly validated in Abbas *et al.* (2015), Abbas and Kornev (2016a) and Abbas and Kornev (2016b). The model of Schnerr and Sauer (2001) was utilized to take the cavitation into account.

3. NUMERICAL IMPLEMENTATION

CFD computations were performed using URANS and hybrid models, utilizing OpenFOAM solver tools developed by Jasak (1996) and Weller *et al.* (1998). The convective term's spatial discretization is achieved through the implementation of the filteredLinear scheme in OpenFOAM.The face values in this method are determined by combining linear interpolation with a specific proportion of the upwind differencing method. The blending ratio depends on the ratio between the gradient within the cell and the gradient across the face. The upwind component is restricted to 20% at most. This filtering approach effectively suppresses high-frequency oscillations, resulting in a stable solution for hybrid and LES simulations, while minimizing unwanted numerical dissipation.

The discretization of the Laplacian term implied with applying a linear method that incorporated an explicit adjustment for non-orthogonality. To reconstruct the pressure gradient, a linear approach

from the Green-Gauss theorem was used. The Crank-Nicolson scheme was used for time discretization. To initialize the flow within the computational domain, the steady RANS solutions were employed.

Computations were performed using a time step of one degree rotation of the propeller, denoted as δt. For cases without cavitation, the unsteady solver pimpleFoam was utilized, while the solver interPhaseChangeDyMFoam was employed for cavitating simulations. The Schnerr and Sauer (2001) model served as the cavitation model. The internal iteration count remained fixed at 50, which proved to be sufficient for achieving convergence.

Geometry is split into stator and rotor components. The rotor includes the propeller and the surrounding domain that undergoes movement over time. To accomplish this, we employed a sliding mesh technique with an arbitrary mesh interface (AMI). The stator pertains to the remaining sections of the domain. Hexpress-Numeca software was used to generate both grids (see Fig. 1).

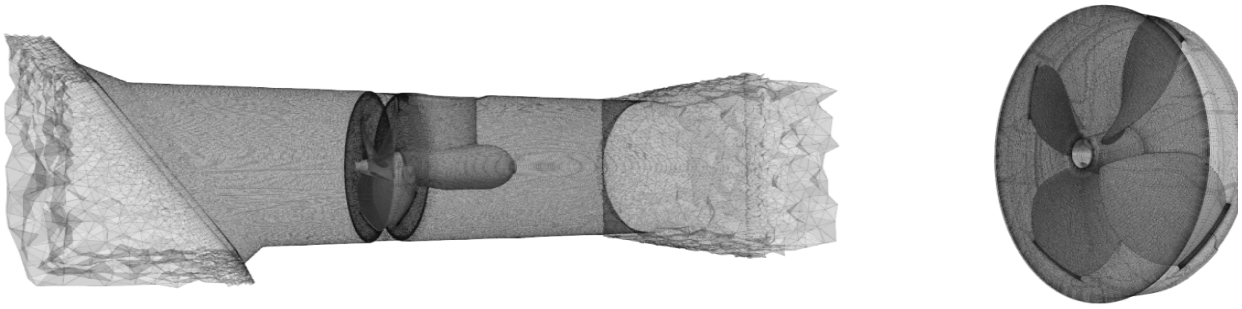

(a) stator (b) rotor

Figure 1: Computational domain

For each element in the tunnel, the target value $y^+ = 45$ has been taken as a basis. Initial estimation of the first cell height was determined using flat plate theory, and a simulation was subsequently conducted. By analyzing the actual y^+ values obtained from the simulation, adjustments were made to the first cell height to achieve the desired $y^+ = 45$ for all elements.

Wall functions have been utilized for viscosity, turbulent kinetic energy (k), and turbulent dissipation rate (ω). Adhering to the logarithmic profile, this approach, based on Menter and Esch (2001), ensures the utilization of a refined near-wall grid.

This analysis reveals that the flow in this scenario displays an unsteady nature, leading to residuals exhibiting semi-periodic patterns. Regardless of the variation for the residuals, the average residual values for velocity, pressure, ω, k, and α during the specified time period are as follows: 10^{-5}, 10^{-4}, 10^{-7}, 10^{-6}, and 10^{-10} respectively. Additionally, the cumulative time continuity error at the end of the simulation time is below 10^{-6}, while generally at each time step it remains below 10^{-9}.

4. Results

Results of verification study (grid independence study) are presented in Fig. 2 for propeller thrust (dashed line with circles), total transverse force (solid line) and propeller torque (dashed line with triangles). The results were obtained using $k-\omega$SST model. As seen from the Figure the monotonic convergence is already achieved for a grid with 18 million cells which is then used for all further calculations.

Validation procedure has been done by comparison of averaged forces with experimental data in **Table 1**. The relative error for any quantity T is defined as $\frac{T_{CFD}-T_{EFD}}{T_{EFD}}$. The results clearly demonstrate that the consideration of cavitation leads to a significant reduction of the deviation between CFD and EFD. Note, that the experimental observations show that the flow has a strong cavitation on propeller blades and, therefore, EFD data correspond to the cavitation case. DDES and URANS with cavitation have errors of seven percent for the propeller thrust, around four percent for the propeller torque and around ten percent for the total transverse force. The results for the SLH model are slightly better: five, one and eight percent, respectively. Taking into account the geometrical complexity of the bow thruster and imperfection of the cavitation model this accuracy can be considered as satisfactory.

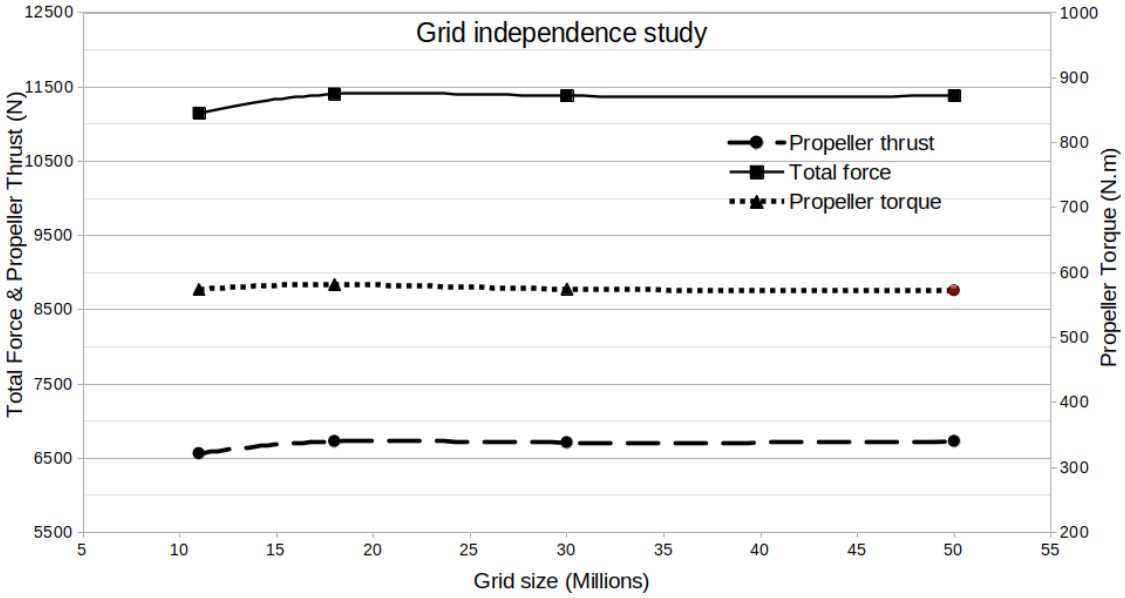

Figure 2: Grid independence study

Table 1: Relative error comparison for time averaged transversal forces and moment

Simulations	Thrust relative error	Torque relative error	Total force
DDES without cavitation	9.82%	1.68%	7.06%
DDES with cavitation	6.91%	3.95%	9.17%
SLH without cavitation	11.17%	-2.64%	6.45%
SLH with cavitation	5.23%	-0.98%	7.72%
URANS without cavitation	10.42%	2.31%	7.45%
URANS with cavitation	6.76%	4.39%	9.65%

Fig. 3 shows the thrust relative error in form of the bar diagram. For all three models, there was a significant decrease in the relative thrust error, if cavitation is taken into account.

Plausibility of scale resolving simulations is often evaluated by analysis of the TKE. The resolved TKE should be at least eighty percent of the total TKE. Fig. 4 represents contour of area with more than 80% resolved TKE. This picture should be analyzed with caution. The change in velocity in rotating flows is due to two reasons. Firstly, the speed fluctuates due to the rotation of the flow caused by the rotating propeller. This part of the velocity fluctuations has nothing to do with turbulence and also

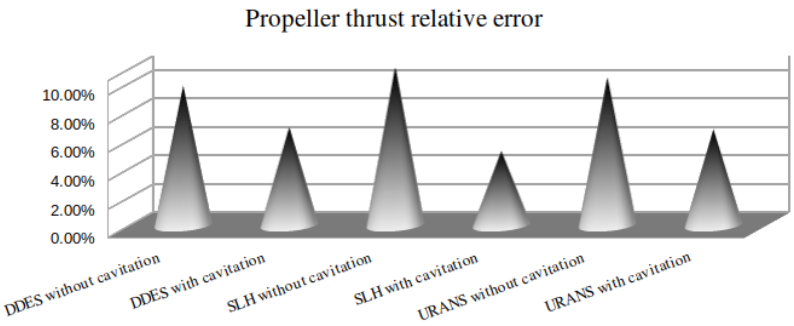

Figure 3: Propeller thrust relative error

exists in laminar flows. The second part of the velocity fluctuations is caused by turbulence. This speed should be taken into account when evaluating resolved TKE. Since the separation of these two components of velocity is not straightforward, this has not yet been done in this paper. Consequently, the torus-like region around the propeller with a predominance of rotation-induced velocities does not allow us to draw reliable conclusions. However, the separation zone in front of the propeller is very informative. In URANS and DES, the 80% resolved TKE in the separation region is not visible, whereas in SLH, the turbulence region with high resolution of TKE is obvious. In other words, SLH resolves high-level turbulence in the separation zone, which is quite expected, while URANS and DDES do not. The reason for the turbulence under resolution by URANS is quite logical and is known from the literature. As for DDES, we found in our previous work (see Anschau*et al.* ((2023)) that the LES branch in DDES is not activated in areas with insufficient turbulence in the incoming flow. It was confirmed in the analysis of the velocity spectrum at different points inside the tunnel which showed that the difference between URANS and DDES is small. This explains similarity between URANS and DDES in Figures 3, 6 and 7. Note that this disadvantage of DDES is typical only for the OpenFOAM implementation whereas the DDES in STAR CCM+ clearly shows the activation of the LES branch with the same grid resolution.

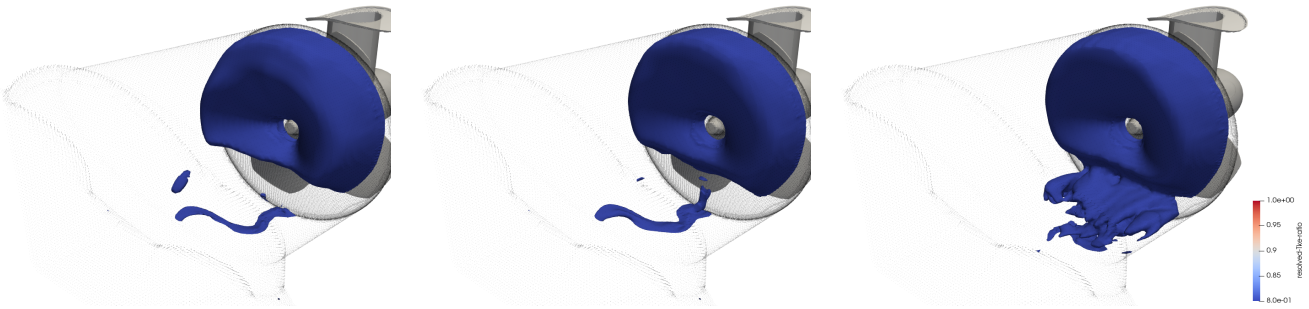

(a) URANS (b) DDES (c) SLH

Figure 4: Area of over 80% resolved turbulent kinetic energy

An additional sign of a proper resolution of turbulence is the presence of the inertial subrange in the velocity spectrum. Fig. 5 illustrates the spectrum for axial velocity at point P5. The dominance of modes corresponding to BPFs is clearly visible. At higher frequencies the reproduction of the inertial subrange with the Kolmogorov $-5/3$ scaling law is observed. As a result, it could be reasoned that LES branch of SLH model in this simulation has been activated, and the grid resolution is sufficient enough to resolve small vortices.

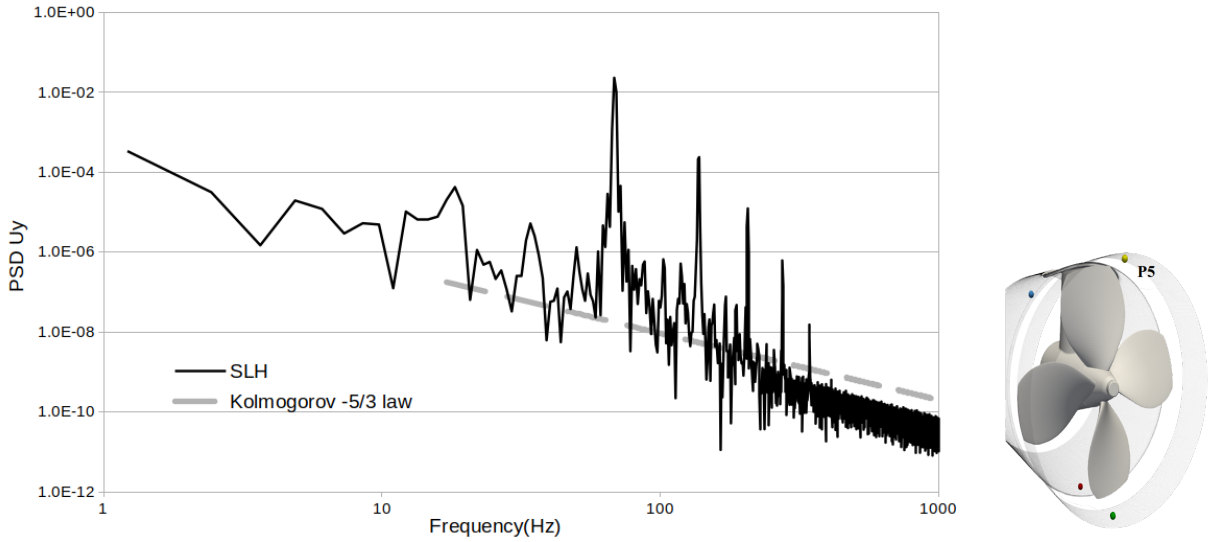

Figure 5: Spectrum of axial velocity in point P5.

Cavitation has a significant effect on the pressure inside the tunnel. Fig. 6 illustrates the magnitude of the mode corresponding to the first blade passing frequency for point P2, which is shown on the right side of the diagram, at the tunnel bottom behind the propeller. The magnitude was obtained from analysis of the pressure's power spectrum density(PSD). For EFD maximum and minimum of the magnitude have been calculated to show the scattering of experimental data. As shown, CFD simulations with account for cavitation agree better with EFD than simulations without cavitation. The pressure obtained without cavitation is much less than the EFD one. Of the three models, only SLH shows results that are between the minimum and maximum EFD values, whereas URANS and DDES results correspond to the maximum EFD. In this respect, the prediction of the SLH model seems to be more reliable. The validation of the first mode shown in Fig. 6 is very important because it makes the greatest contribution to the noise emission and vibrations of the bow thrusters.

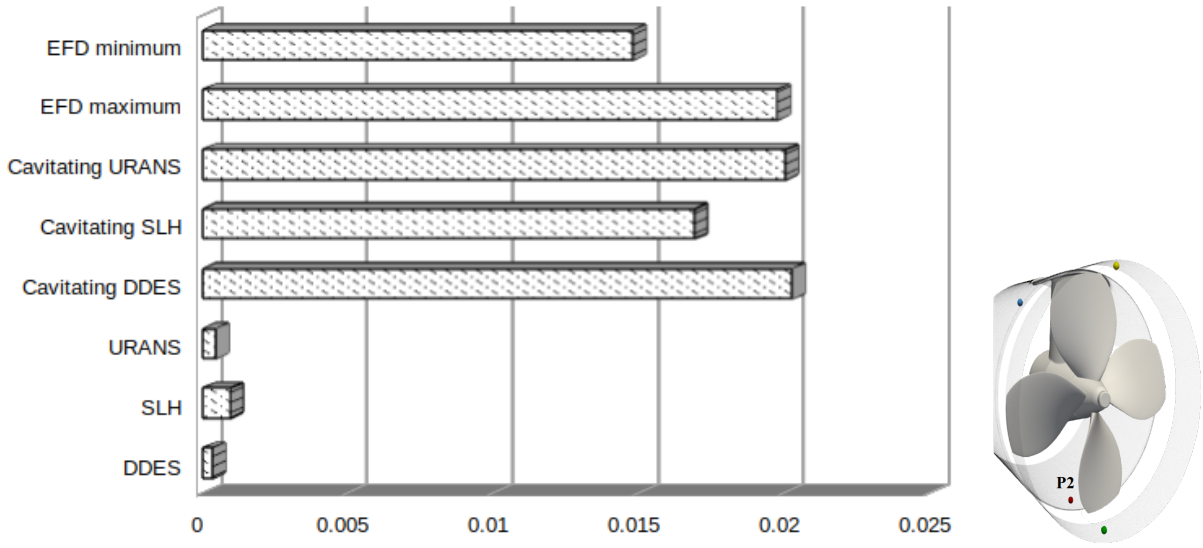

Figure 6: Magnitude of the mode corresponding to the first blade passing frequency at point P2.

Unsteady loading on the propeller are illustrated with the root mean square of the thrust fluctuation $\sqrt{\overline{(T(t)-T_{mean})^2}}$ referred to the mean thrust T_{mean}

$$\tilde{T'} = \frac{T'}{T_{mean}} = \frac{\sqrt{\overline{(T(t)-T_{mean})^2}}}{T_{mean}} \tag{4}$$

in Fig. 7. As expected, cavitation makes a great contribution to the thrust fluctuations. The cavitation results in increase of $\tilde{T'}$ and, consequently, in enhancement of unsteady loading on the propeller. Overshoot of the pressure magnitude obtained using URANS and DDES models with cavitation (see Fig. 6) is also reflected in the increase in thrust fluctuations in URANS and DDES predictions. The referred thrust fluctuations $\tilde{T'}$ in URANS and DDES is about two percent higher than in SLH simulations. Without cavitation the SLH results are higher than URANS and DDES ones. All CFD results reveal substantial thrust fluctuations of the bow thruster propeller which are in the range between ten and thirteen percent for non cavitating propeller and around sixteen and eighteen percent for the case with cavitation. This fluctuation is much higher than the thrust fluctuation on conventional propeller which is, for example, between two and three percent for the non cavitating propeller behind the tanker KVLCC2 (see, for example, Abbas *et al.* (2015)). As is known, the unsteady forces on the hull caused by the propeller are divided into two parts: the forces transmitted from the propeller to the hull through the propeller shaft, and the forces transmitted through the water due to unsteady pressure pulsations on the hull caused by the propeller. The results shown in Fig. 7 clearly demonstrate that the first part of the unsteady forces is very high for bow thrusters. This explains the increased vibration level observed when the bow thruster is turned on during maneuvering. Also the second part of forces caused by pressure fluctuations on thruster tunnel walls makes a substantial contribution to vibrations and acoustic emission.

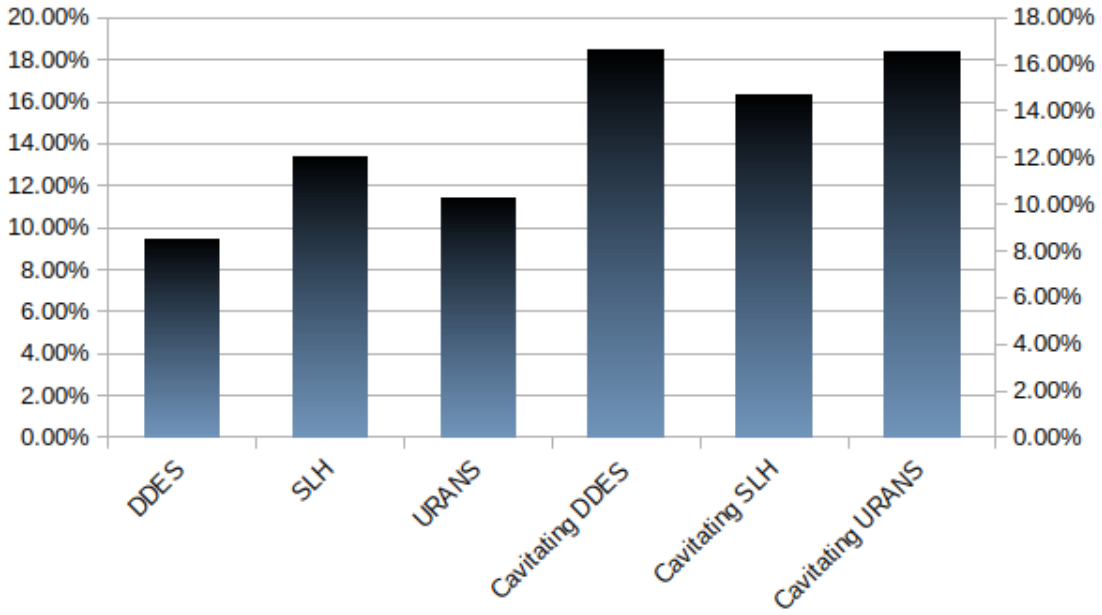

Figure 7: Ratio of the mean thrust fluctuation to the mean thrust $\tilde{T'}$.

5. CONCLUSIONS

Scale resolving simulation is able to properly reproduce steady and unsteady hydrodynamic effects in bow thrusters. The error of CFD prediction of the propeller thrust and torque doesn't exceed five percent when the SLH hybrid model is utilized. Agreement between CFD and EFD is substantially improved when the cavitation is taken into account.

CFD study confirmed increase of thrust fluctuations in comparison with conventional propellers which explains the increase of vibrations when bow thruster is turned on during maneuvering. More precisely the mean thrust fluctuation referred to the mean thrust can achieve the range between sixteen and eighteen percent whereas it does not exceed three percent for conventional propellers.

ACKNOWLEDGEMENTS

The authors acknowledge gratefully the support of the German Federal Ministry for Economic Affairs and Climate Action within the framework of the project 03SX530E monitored by Dr. J. Turnow. The authors also thank Jastram GmbH & Co. KG (Dr. Jörn Hinnenthal) for providing geometric and experimental data for their bow thruster.

AUTHOR'S CONTRIBUTION

MK performed the compuations and wrote a part of manuscript. NK supervised and coordinated the project as well as wrote the manuscript. All authors edited and approved the manuscript.

REFERENCES

Anschau, P., Kornev, N. and Samarbakhsh, P. (2023). Unsteady hydrodynamic loads on energy saving ducts, *Ocean Engineering*, 269, https://doi.org/10.1016/j.oceaneng.2022.113431.

Abbas, N., Kornev, N., Shevchuk, I. and Anschau, P. (2015). CFD prediction of unsteady forces on marine propellers caused by the wake nonuniformity and nonstationarity, *Ocean Engineering*, 104, 659–672.

Abbas, N. and Kornev, N. (2016a). Study of unsteady loadings on the propeller under steady drift and yaw motion using URANS, hybrid (URANS-LES) and LES methods, *Ship Technology Research*, 63 (2), 121–131.

Abbas, N. and Kornev, N. (2016b). Validation of hybrid URANS/LES methods for determination of forces and wake parameters of KVLCC2 tanker at maneuvering conditions, *Ship Technology Research*, 63 (2), 96–109.

Bagrintsev, V., Koval, A. and Marinich, N. (2019). Optimization of thruster propeller geometry to mitigate periodical forces, *Transaction of the Krylov State Research Centre*, Special Edition 2, 67–72.

Brizzolara, S. and Brizzolara, E. (2017). Long Tunnel Configurations for High Efficiency Thrusters, *Proc. 5th Int. Symp. Marine Propulsors SMP'17*, Espoo, Finland.

Ermolaev, A. and Shevtsov, S. (2018). Vibration of thrusters and ways to combat it, *Transaction of the Krylov State Research Centre*, Special issue 1, 67–74.

Jasak, H. (1996). Error analysis and estimation for the finite volume method with applications to

fluid flows, PhD thesis, Imperial College of Science, Technology and Medicine, London.

Kornev, N., Taranov, A., Shchukin, E. and Kleinsorge, L. (2011). Development of hybrid URANS-LES methods for flow simulation in the ship stern area, *Ocean Engineering*, 38(16), 1831–1838.

Menter, F.R. (1994). Two-equation eddy-viscosity turbulence models for engineering applications, *AIAA journal*, 32(8), 1598–1605.

Menter, F. R. and Esch, T. (2001). Elements of industrial heat transfer predictions, *16th Brazilian Congress of Mechanical Engineering (COBEM)*, Uberlandia, Brazil.

Mohan, A. (2017). Numerical Analysis of Bow Tunnel Thruster Performance, Master thesis, TU Delft.

Ozdemir, Y. , Bayraktar, S., Yilmaz, T. and Guner, M. (2008). Determining optimum geometry for a bow thruster propeller, https:// www.researchgate.net/ publication/ 288705948.

Schnerr, G.H. and Sauer, J. (2001) Physical and Numerical Modeling of Unsteady Cavitation Dynamics. *4th International Conference on Multiphase Flows*.

Shevchuk, I. and Kornev, N. (2018). Improved version of LeMos Hybrid Model for Ambiguous Grid Densities, *International Journal of Naval Architecture and Ocean Engineering*, 10 (3), 270–281.

Shevtsov S. (2014). Investigation of hydrodynamic characteristics of thrusters of the "screw in the pipe" type. Clarification of the design methodology of these devices, including high power installations. PhD thesis, Krylov Research Centre, St. Petersburg, Russia (in Russian).

Shur, M., Spalart, P., Strelets, M. and Travin, A. (2008) A hybrid RANS-LES approach with delayed-DES and wall- modelled LES capabilities, *Int. J. Heat and Fluid Flow*, YEAR = 2008, 29 (6), 1638–1649.

Yao, Z. and Yan, Z. (2012). Hydrodynamic performance analysis and verification of transverse thrusters, *Journal of Ship Mechanics* , 16 (3), 236–245.

Yu, C. and Yang, C. (2016). Study of Tunnel Thruster Performance and Flow by Quasi-Steady Reynolds-Averaged Navier-Stokes Simulation, *J. Shanghai Jiaotong Univ. (Sci.)*, 21 (6), 662–671.

Weller, H. G. and Tabor, G. and Jasak, H. and Fureby, C. (1998). A tensorial approach to computational continuum mechanics using object-oriented techniques, *Computers in Physics*, 12 (6), 620–631.